


# Superconducting anisotropy and vortex pinning in $CaKFe_4As_4$ and $KCa_2Fe_4As_4F_2$

A B Yu(于奥博), Z Huang(黄喆), C Zhang(张驰), Y F Wu(吴宇峰), T Wang(王腾), T Xie(谢涛), C Liu(刘畅), H Li(李浩), W Peng(彭炜), H Q Luo(罗会仟), G Mu(牟刚), H Xiao(肖宏), L X You(尤立星), and T Hu(胡涛)

**Citation:**Chin. Phys. B, 2021, 30 (**2**): 027401. DOI: 10.1088/1674-1056/abcf98
Journal homepage: http://cpb.iphy.ac.cn; http://iopscience.iop.org/cpb

**What follows is a list of articles you may be interested in**

---

## Phase-field simulation of superconductor vortex clustering in the vicinity of ferromagnetic domain bifurcations

Hasnain Mehdi Jafri, Jing Wang(王静), Chao Yang(杨超), Jun-Sheng Wang(王俊升), and Hou-Bing Huang(黄厚兵)
Chin. Phys. B, 2020, 29 (**12**): 127402. DOI: 10.1088/1674-1056/abb22c

## Anisotropy of $Ca_{0.73}La_{0.27}(Fe_{0.96}Co_{0.04})As_2$ studied by torque magnetometry

Ya-Lei Huang(黄亚磊), Run Yang(杨润), Pei-Gang Li(李培刚), Hong Xiao(肖宏)
Chin. Phys. B, 2020, 29 (**9**): 097405. DOI: 10.1088/1674-1056/ab9f26

## Specific heat in superconductors

Hai-Hu Wen(闻海虎)
Chin. Phys. B, 2020, 29 (**1**): 017401. DOI: 10.1088/1674-1056/ab5a3d

## Vortex pinning and rectification effect in a nanostructured superconducting film with a square array of antidot triplets

An He(何安), Cun Xue(薛存), Youhe Zhou(周又和)
Chin. Phys. B, 2018, 27 (**5**): 057402. DOI: 10.1088/1674-1056/27/5/057402

## Magneto-resistance and vortex phase diagram of $BaNi_{0.1}Fe_{1.9}As_2$ single crystal

Lu Jun-Chao, Yu Yi, Pi Li, Zhang Yu-Heng
Chin. Phys. B, 2014, 23 (**12**): 127402. DOI: 10.1088/1674-1056/23/12/127402

---

RAPID COMMUNICATION

# Superconducting anisotropy and vortex pinning in $CaKFe_4As_4$ and $KCa_2Fe_4As_4F_2$*

A B Yu(于奥博)[1,4,5], Z Huang(黄喆)[1,4], C Zhang(张驰)[1,4,5], Y F Wu(吴宇峰)[2], T Wang(王腾)[1,4], T Xie(谢涛)[5,6], C Liu(刘畅)[5,6], H Li(李浩)[1,4,5], W Peng(彭炜)[1,4,5], H Q Luo(罗会仟)[5,6,7], G Mu(牟刚)[1,4,5], H Xiao(肖宏)[3], L X You(尤立星)[1,4,5], and T Hu(胡涛)[2,†]

[1] *State Key Laboratory of Functional Materials for Informatics, Shanghai Institute of Microsystem and Information Technology, Chinese Academy of Sciences, Shanghai* 200050, *China*

[2] *Beijing Academy of Quantum Information Sciences, Beijing* 100193, *China*

[3] *Center for High Pressure Science and Technology Advanced Research, Beijing* 100094, *China*

[4] *CAS Center for Excellence in Superconducting Electronics (CENSE), Shanghai* 200050, *China*

[5] *University of Chinese Academy of Sciences, Beijing* 100049, *China*

[6] *Beijing National Laboratory for Condensed Matter Physics, Institute of Physics, Chinese Academy of Sciences, Beijing* 100190, *China*

[7] *Songshan Lake Materials Laboratory, Dongguan* 523808, *China*

(Received 26 October 2020; revised manuscript received 27 November 2020; accepted manuscript online 2 December 2020)

The vortex pinning determining the current carrying capacity of a superconductor is an important property to the applications of superconducting materials. For layered superconductors, the vortex pinning can be enhanced by a strong interlayer interaction in accompany with a suppression of superconducting anisotropy, which remains to be investigated in iron based superconductors (FeSCs) with the layered structure. Here, based on the transport and magnetic torque measurements, we experimentally investigate the vortex pinning in two bilayer FeSCs, $CaKFe_4As_4$(Fe1144) and $KCa_2Fe_4As_4F_2$(Fe12442), and compare their superconducting anisotropy $\gamma$. While the anisotropy $\gamma \approx 3$ for Fe1144 is much smaller than $\gamma \approx 15$ in Fe12442 around $T_c$, a higher flux pinning energy as evidenced by a higher critical current density is found in Fe1144, as compared with the case of Fe12442. In combination with the literature data of $Ba_{0.72}K_{0.28}Fe_2As_2$ and $NdFeAsO_{0.82}F_{0.18}$, we reveal an anti-correlation between the pinning energy and the superconducting anisotropy in these FeSCs. Our results thus suggest that the interlayer interaction can not be neglected when considering the vortex pinning in FeSCs.

**Keywords:** iron based superconductors, vortex pinning, anisotropy

**PACS:** 74.25.Qt, 75.30.Gw, 74.25.Sv **DOI:** 10.1088/1674-1056/abcf98

## 1. Introduction

Vortex pinning governing the critical current density ($J_c$) is crucial to the practical applications of superconducting materials. $J_c$ is defined as the maximum electrical current density that sustains superconductivity without resistance, that is, increasing the current density beyond $J_c$ will lead to the depinning of the vortices and consequently to the disappearance of zero resistance. The study of vortex pinning and $J_c$ enhancement is therefore carried out intensively.[1–4] In a real superconductor, vortex pinning is closely related to the defect structure in the material and the properties of the vortex matter.[1] Thus one can improve the value of $J_c$ by the fabrication of superlattices,[5] irradiation,[6,7] and introduction of stacking faults.[8] In particular, for high temperature cuprate superconductors, the layered structure has a dramatic influence on properties of the vortex matter.[1,9] Pancake vortices arise in each $CuO_2$ layer of cuprates, the interaction between which is found to enhance the vortex pinning.[9,10] For a material with weak interlayer interaction, the superconductivity is highly anisotropic and the vortex line is highly flexible, which can be deformed easily. While in the strong interlayer interaction case, the superconductor has moderately anisotropic vortices.[9,10] Consequently, the interlayer interaction determines superconducting anisotropy and significantly affects the $J_c$ in layered structure superconductors.[1,9]

The iron based superconductors (FeSCs) are a new class of high transition temperature ($T_c$) superconductors[11,12] with a generally smaller superconducting anisotropy than cuprates. This system attracts a lot of research interest because of its outstanding properties[13,14] like high $T_c$, large upper critical field, and high $J_c$. Similar to cuprates, FeSCs reveal a layered structure, with FeAs superconducting layers alternating

*Project supported by the National Natural Science Foundation of China (Grant No. 11574338) and the National Natural Science Foundation of China–China Academy of Engineering Physics NSAF Joint Fund (Grant No. U1530402). The experimental measurements were supported by the Superconducting Electronics Facility (SELF) of Shanghai Institute of Microsystem and Information Technology. The work at IOP, CAS was supported by the National Key Research and Development Program of China (Grant No. 2018YFA0704200), the National Natural Science Foundation of China (Grant Nos. 11822411 and 11961160699), the Strategic Priority Research Program (B) of the Chinese Academy of Sciences (CAS) (Grant No. XDB25000000), and the Youth Innovation Promotion Association of CAS (Grant No. 2016004).

†Corresponding author. E-mail: hutao@baqis.ac.cn

© 2021 Chinese Physical Society and IOP Publishing Ltd 

with the insulating layers or other conducting layers, which leads to the different anisotropy among different systems.[15] For example, in the bilayer FeSC $CaKFe_4As_4$ (Fe1144), FeAs layers are separated by Ca and K atoms along $c$ axes,[16] which leads to a small anisotropy $\gamma \approx 3$ near $T_c$.[17,18] Meanwhile, a high $J_c$,[19,20] combined with the high upper critical field[17] and the unconventional superconductivity,[19] is also observed in Fe1144. In contrast, in another newly discovered bilayer FeSC $KCa_2Fe_4As_4F_2$ (Fe12442), the FeAs layers are alternately separated by conductive K and insulating $CaF_2$ layers,[21] which results in a relatively weaker interlayer interaction than that in Fe1144. The properties of 12442 family[22–25] are close to those of bilayer cuprates and it is a well connector between FeSCs and cuprates. Our previous work[26,27] showed that the $\gamma$ of Fe12442 is $\sim 15$ near $T_c$, which is much larger than that of Fe1144. Such distinct superconducting anisotropies in these two bilayer systems provide an unique opportunity to understand the role of interlayer interaction in the vortex pinning of FeSCs.

In this article, detailed electrical transport and angular dependent torque measurements are carried out on Fe1144 and Fe12442 single crystals at various temperatures and magnetic fields. The resistance measurements show that the anisotropy parameter of upper critical field $\gamma = H_{c2}^{ab}/H_{c2}^{c}$ is about 3 for Fe1144, which is less than $\gamma \approx 15$ for Fe12442 at $T \to T_c$. While the pinning energy of Fe1144 is much larger than that of Fe12442 according to the analysis of the thermal activated flux flow (TAFF) behavior. In addition, torque measurements further confirm the results observed in transport measurements. From the fitting results of reversible torque by Kogan's model, we find that anisotropy $\gamma$ determined from the penetration depth is about 3 for Fe1144 and 15 for Fe12442 near $T_c$, respectively. The value of critical current density $J_c$ is calculated from the irreversible component of the magnetic torque, which provides evidence for a higher $J_c$ in Fe1144 than Fe12442. Furthermore, in combination with the literature data of other FeSC systems, $Ba_{0.72}K_{0.28}Fe_2As_2$ and $NdFeAsO_{0.82}F_{0.18}$, we show that a stronger vortex pinning occurs in those FeSCs which have a smaller anisotropy. Our results suggest that the interlayer interaction may play a crucial role in vortex pinning of Fe12442 and Fe1144.

## 2. Experiment

The single crystals of $CaKFe_4As_4$ and $KCa_2Fe_4As_4F_2$ are grown by using the self-flux method.[17,28,29] Sharp superconducting transition at $T_c$ in resistance and magnetization measurements shows a high-quality of our single crystal samples. The angular ($\theta$) dependent torque is measured at different temperatures and applied magnetic fields by using piezoresistive torque magnetometer in the Quantum Design physical property measurement system (PPMS). $\theta$ is the angle between the applied field and $c$ axes of the single crystal. The temperature dependent 4-wire resistance measurements are performed by the resistance bridge options of PPMS with $0\ \mathrm{T} \le H \le 9\ \mathrm{T}$ at a heating rate 1 K/min. The magnetic moment measurements are carried out by using magnetic property measurement systems (MPMS) with $H = 10$ Oe applied along $c$ axes of the single crystal. The transport data of Fe12442 in the paper are taken from our previous work.[26]

## 3. Results and discussion

Figure 1 shows the transport properties of single crystal $CaKFe_4As_4$ (Fe1144). The temperature ($T$) dependent resistances of Fe1144 measured at applied magnetic fields $H$ along $c$ and in-plane crystalline directions are shown in Figs. 1(a) and 1(b), respectively. As cooling down, the resistance decreases suddenly at the temperature $T_c$ and drop to zero resistance at lower temperature as a result of the superconducting transition. The transition is very sharp at zero field, which becomes broader with increasing $H$. It is found that the transition with $H \parallel c$ is broader than that with $H \parallel ab$ under the same values of $H$, which suggests the presence of anisotropic superconductivity in Fe1144. In

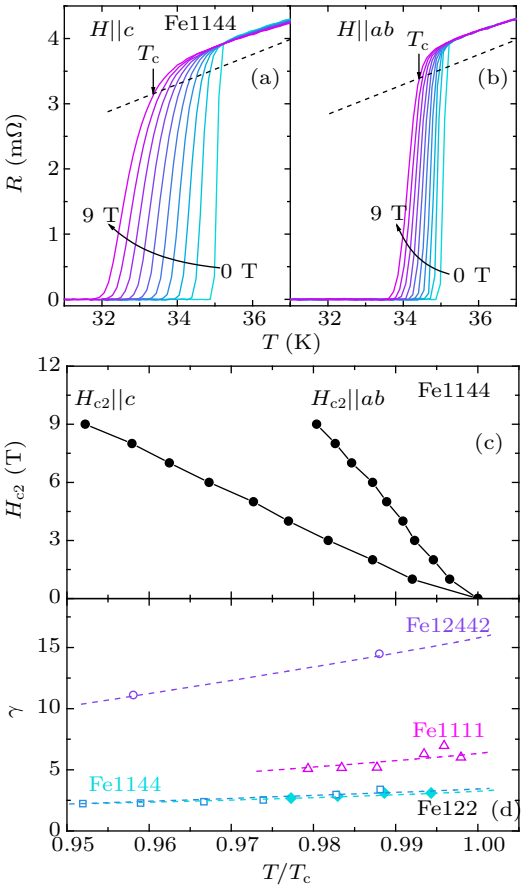



**Fig. 1.** Temperature $T$ dependence of resistance $R$ of $CaKFe_4As_4$ at different applied magnetic fields $H$ with $H \parallel c$ (a) and $H \parallel ab$ (b). (c) $T$ dependent of upper critical field $H_{c2}$ for $CaKFe_4As_4$ at $H \parallel c$ and $H \parallel ab$. (d) The upper critical field anisotropy parameter $\gamma = H_{c2}^{ab}/H_{c2}^{c}$ of $CaKFe_4As_4$, $KCa_2Fe_4As_4F_2$,[26] $Ba_{0.72}K_{0.28}Fe_2As_2$,[15] and $NdFeAsO_{0.82}F_{0.18}$.[30] The dashed lines are guides to the eyes.

order to study the anisotropy quantitatively, we define the upper critical field of $H_{c2}$ or $T_c(H)$ at the position where the resistance arrives at 90% of its normal state value as shown by the arrows in Figs. 1(a) and 1(b). Figure 1(c) shows the upper critical field out-of-plane ($H_{c2}^{c}$) and in-plane directions ($H_{c2}^{ab}$) of Fe1144. Figure 1(d) displays the anisotropy of upper critical field $\gamma = H_{c2}^{ab}/H_{c2}^{c}$ for Fe1144 and the literate data for Fe12442,[26] $Ba_{0.72}K_{0.28}Fe_2As_2$ (Fe122),[15] and $NdFeAsO_{0.82}F_{0.18}$ (Fe1111).[30] In the anisotropic Ginzburg–Landau (GL) theory, the anisotropic parameter is defined as $\gamma = \sqrt{m_c^*/m_{ab}^*} = \lambda_c/\lambda_{ab} = H_{c2}^{ab}/H_{c2}^{c} = \xi_{ab}/\xi_c$, where $ab$ and $c$ denote the orientations along the crystal, $m^*$ is the effective mass, $\lambda$ is the penetration depth, and $\xi$ is the coherence length.[31] Figure 1(d) thus suggests that the largest superconducting anisotropy arises in Fe12442, the moderate anisotropy in Fe1111, and the smallest anisotropy in Fe1144 and Fe122. It is worth noting that here we use the $\gamma$ values near $T_c$ to make the comparisons among different FeSCs. Such a comparison was previously performed in FeSCs,[32] to avoid the influences of other factors, like the anisotropic paramagnetic effects,[33,34] on $\gamma$ at the low temperatures.

In order to investigate the correlation between superconducting anisotropy and vortex pinning, we study the thermally activated flux-flow (TAFF) behavior in FeSCs. Based on the TAFF model $\rho(H,T) = \rho_0 \exp(-U/k_B T)$, one can acquire the thermal activation energy $U$ from the slope of liner portion of Arrhenius plot $\ln(\rho/\rho_0)$ versus $T^{-1}$, where $\rho_0$ is a factor independent of the magnetic field and $k_B$ is the Boltzmann constant. Figures 2(a) and 2(b) show the resistance Arrhenius plots of Fe1144 and Fe12442 single crystals for magnetic field along $c$-axes of the samples with 1 T $\leq H \leq$ 9 T. The obtained thermal activation energy $U$ at different magnetic fields is shown in Fig. 2(c), along with that of Fe1111 and Fe122.[15,35] The relationship of $\gamma$ and $U$ for four single crystals is plotted in Fig. 2(d). Error bars are given by mean deviation. Figure 2(d) shows that the average $U$ in the investigated $H$ range of these FeSCs samples is anti-correlated with their superconducting anisotropy $\gamma$. For Fe12442 and Fe1144, the anti-correlated relation is independent of samples as shown in Fig. A1. Interestingly, such an anti-correlated relationship was also observed at $T = 0$ K in series $BaFe_{2-x}Ni_xAs_2$, where the one that exhibits the maximum $J_c$[36] has the smallest $\gamma$.[37] In general, many factors, such as disorder landscape, defect, and other material parameters, have important influences on vortex pinning of superconductors. However, the revealed anti-correlated relationship between $U$ and $\gamma$ here suggests that the interlayer interaction can not be neglected in vortex pinning in FeSCs. In addition, it is worth noting that the anisotropy of Fe1144 is almost the same as that of Fe122 while the pinning energy of Fe1144 is slightly larger than that of Fe122 as shown in Fig. 2(d). It may reflect that besides the interlayer interaction, the unique inherent defect structure of Fe1144 also significantly enhances the $J_c$.[20]

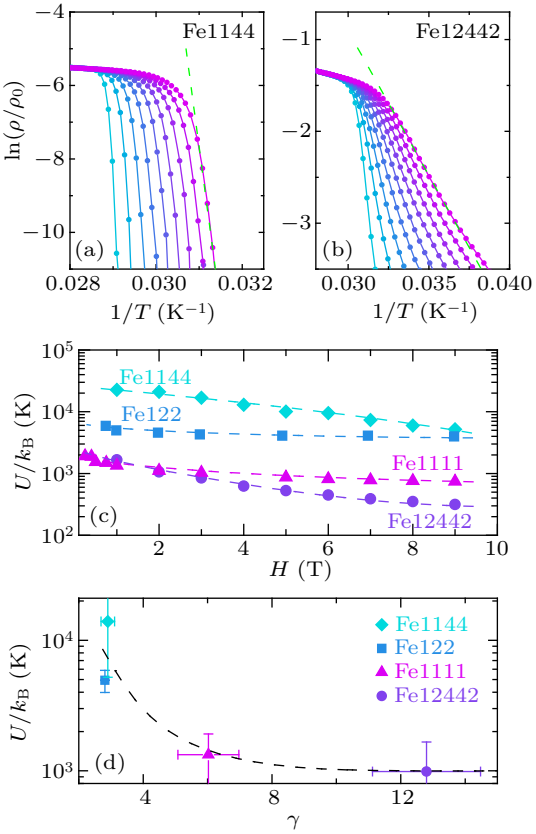



**Fig. 2.** Arrhenius plots obtained from $R$ vs. $T$ under $H \parallel c$ for $CaKFe_4As_4$ (a) and $KCa_2Fe_4As_4F_2$ (b). (c) The $H$ dependence of thermal activation energy $U$ for Fe1144 (our data), Fe12442 (our data), Fe122,[15] and Fe1111.[35] (d) The $\gamma$ vs. $U$. Error bars are mean deviation and the dash lines are guides to the eyes.

Furthermore, compared with the transport measurements, magnetic torque is sensitive to the magnetic anisotropy of materials. By using torque measurements, one can obtain the superconductivity anisotropy $\gamma$ and $J_c$ simultaneously. That is, the reversible part of magnetic torque reflects the equilibrium state and is determined by the thermodynamic parameters and their anisotropy,[38] while the irreversible part reflects the non-equilibrium state resulting from vortex pinning, whose amplitude is governed by the critical current density $J_c$.[39,40]

The torque of a sample with magnetic moment $M$ in magnetic field $H$ can be expressed as

$$\boldsymbol{\tau} = \boldsymbol{M} \times \boldsymbol{H}. \tag{1}$$

For the anisotropic materials whose moment and field are non-collinear, the magnitude of torque is[31]

$$\tau(\theta) = V\left(M_c H_{ab} - M_{ab} H_c\right), \tag{2}$$

where $V$ is the volume of the sample, the magnetization and field along $a$ and $c$ axes are presented as $M_c$, $M_{ab}$, $H_c$, $H_{ab}$, which can be derived by using vortex lattice Helmholtz free energy[41] accompanying with $\boldsymbol{H} = 4\pi(\partial F/\partial \boldsymbol{B}) = \boldsymbol{B} - 4\pi\boldsymbol{M}$.[31,38] Considering the facts that $\boldsymbol{M}$ is non-collinear

with $\boldsymbol{B}$ and $|\boldsymbol{M}| \ll |\boldsymbol{B}|$, $\boldsymbol{B} \approx \boldsymbol{H}$, the concrete form of the vortex torque $\tau_v(\theta)$ can be written as

$$\tau_v(\theta) = \frac{\phi_0 HV}{64\pi^2\lambda_{ab}^2}\frac{\gamma^2-1}{\gamma}\frac{\sin 2\theta}{\varepsilon(\theta)}\ln\left\{\frac{\gamma\eta H_{c2}^c}{H\varepsilon(\theta)}\right\}, \qquad (3)$$

which is the so called Kogan's model,[38] where $\varepsilon(\theta) = \sqrt{\sin^2\theta + \gamma^2\cos^2\theta}$. Thus one can obtain the anisotropy $\gamma$ through fitting the reversible part of vortex torque with this formula.

Figure 3(a) shows the typical $\tau(\theta)$ curves of Fe1144 measured at normal state ($T > T_c$), where $\theta$ is the angle between the applied magnetic field $H$ and $c$ axis of the sample. It is found that $\tau(\theta)$ (open circles) can be fitted well by the equation $A\sin 2\theta$ (solid lines). Therefore, the value of $A$ represents the amplitude of the $\tau(\theta)$ curves at normal state and equals to the torque measured at $\theta = 45°$. The field $H$ dependence of $-A$ measured at $T = 45$ K and 60 K is displayed in Fig. 3(b). The parameter $-A$ shows a linear relationship with $H^2$, which is the feature of the paramagnetic torque in the normal state. The paramagnetic torque is $\tau_p = \frac{\chi_c-\chi_a}{2}H^2\sin 2\theta$, which is determined by the difference of susceptibility along $a$-axes ($\chi_a$) and $c$-axes ($\chi_c$).[42,43] Note that the value of $A$ is negative in Fig. 3(b). It suggests that the $\chi_c$ is smaller than $\chi_a$, which is also observed in other systems of FeSCs.[44,45] This is different from cuprate superconductor $Bi_2Sr_{2-x}La_xCuO_{6+\delta}$[46] and heavy fermion superconductor $CeCoIn_5$,[47] where $\chi_c$ is larger than $\chi_a$. In addition, the parameter $A$ measured at $T = 45$ K is almost coincided with that at $T = 60$ K, suggesting that the paramagnetic torque is nearly constant at $T > T_c$ with the same magnetic field as also shown in Fig. 3(c).

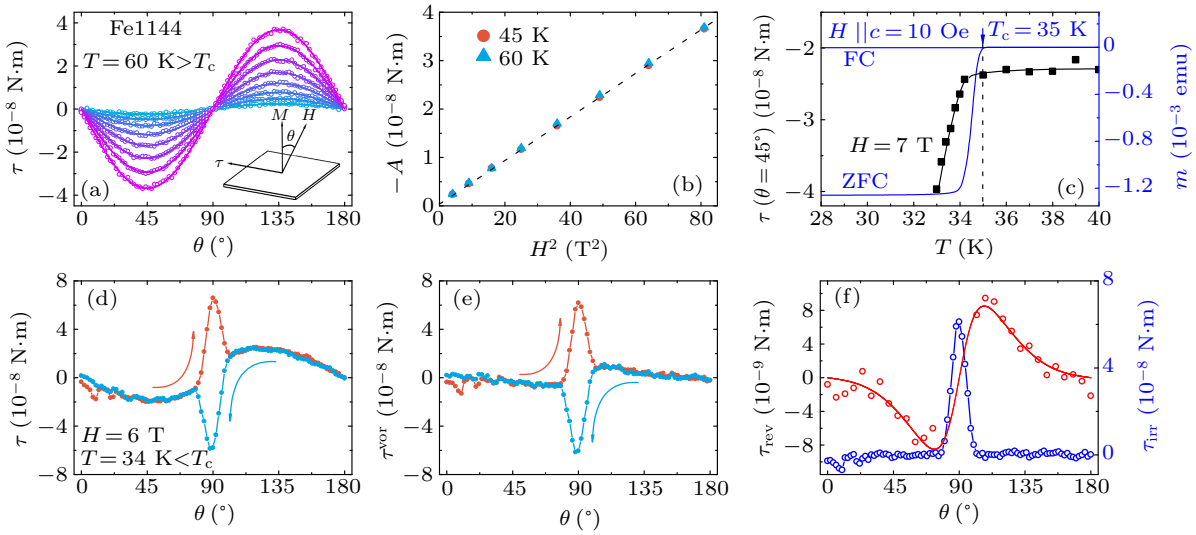



**Fig. 3.** The torque data of Fe1144. (a) The typical angular $\theta$ dependent torque data $\tau$ (hollow circles) at $T = 60$ K with $H = 2$–9 T and the fitting results (solid lines) by $A\sin 2\theta$. Inset to (a) shows the orientation of $H$, $\tau$, and crystallographic axes. (b) Parameter $-A$ vs. $H^2$ at $T = 45$ K and 60 K. (c) Left axis: $T$ dependence of $\tau(\theta = 45°)$ at $H = 7$ T. Right axis: the magnetization data at $H \parallel c = 10$ Oe under zero field cooling (ZFC) and field cooling (FC) conditions. (d) $\theta$ dependence of $\tau$ measured at $T = 34$ K and $H = 6$ T with increased $\theta$ ($\tau_{inc}$) and decreased $\theta$ ($\tau_{dec}$). (e) $\theta$ dependence of vortex torque $\tau^{vor}$ at $T = 34$ K, $H = 6$ T after subtracting the normal state torque. (f) $\theta$ dependence of reversible torque $\tau_{rev} = (\tau_{inc}^{vor} + \tau_{dec}^{vor})/2$ (left axis) and irreversible torque $\tau_{irr} = (\tau_{inc}^{vor} - \tau_{dec}^{vor})/2$ (right axis). The red line is the fitting curve according to Kogan's formula.

Figure 3(c) (left axis) shows $T$ dependence of $\tau(\theta = 45°)$ of Fe1144 single crystal with $H = 7$ T. It is found that $\tau(\theta = 45°)$ keeps almost constant above $T_c = 35$ K but then drops quickly below $T_c$. The drop of $\tau(\theta = 45°)$ below $T_c$ can be understood in terms of the arise of vortex torque ($\tau^{vor}$) in the mixed state. The magnitude of the vortex torque can be obtained by subtracting the normal state torque since the paramagnetic torque is nearly constant at $T > T_c$ as shown in Figs. 3(b) and 3(c). Here, $T_c$ is determined by magnetization measurements ($m$) in low magnetic field $H = 10$ Oe applied along the $c$-axis of Fe1144 as shown in Fig. 3(c) (right axis), at which a large diamagnetization arises in zero-field cooled (ZFC) magnetization curve, while the field-cooled (FC) magnetization keeps unchanged. Figure 3(d) shows the torque data measured at $T = 34$ K $< T_c$ and $H = 6$ T with increasing angle $\tau_{inc}$ and decreasing angle $\tau_{dec}$. A large torque hysteresis loop can be found around 90°, which is caused by the intrinsic pinning[48–50] owing to the layered structure of the superconductors.

Furthermore, the vortex torque $\tau^{vor}$ can be obtained by removing the torque at normal state as discussed above, $\tau^{vor}(T,\theta) = \tau(T,\theta) - A(T = 60\ \text{K})\sin 2\theta$, which is shown in Fig. 3(e). In order to investigate the anisotropy and flux pinning, $\tau^{vor}$ has to be separated into the reversible component $\tau_{rev} = (\tau_{inc}^{vor} + \tau_{dec}^{vor})/2$ and the irreversible component $\tau_{irr} = (\tau_{inc}^{vor} - \tau_{dec}^{vor})/2$ as shown in Fig. 3(f). Note that only the reversible part reflecting the equilibrium state can be described by Kogan's model. We therefore fit the angle dependence of $\tau_{rev}$ by Eq. (3) with fitting parameters $C$ and $\gamma$, where $C = \frac{\phi_0 HV}{64\pi^2\lambda_{ab}^2}$. The fitting result is displayed by the red solid line in Fig. 3(f). In the mean time, $\tau_{irr}(\theta)$ shows a sharp peak around 90° as represented by the blue curve in Fig. 3(f).

Such a $\tau_{irr}(\theta)$ behavior was also observed in cuprate superconductor $Bi_2Sr_2CaCu_2O_x$ and interpreted as the result of vortex pinning.[39] Detailed analysis of $\tau_{rev}$ and $\tau_{irr}$ for Fe1144 and Fe12442 single crystals is shown in Figs. A2 and A3.

The $H$ and $T$ dependences of anisotropy parameter $\gamma$ for Fe1144 and Fe12442 are summarized in Figs. 4(a) and 4(b), respectively. Error bars are defined as the uncertainty of fit. It is found that $\gamma$ almost stays constant within the investigated temperature and field ranges. For Fe1144, the value of $\gamma \approx 3$ at $T \to T_c$ agrees with the result of muon-spin rotation measurement.[18] Thus, the Fe1144 system shows much smaller anisotropy than Fe12442 whose $\gamma \sim 15$ around $T_c$,[27] which is consistent with the results from the transport measurements.

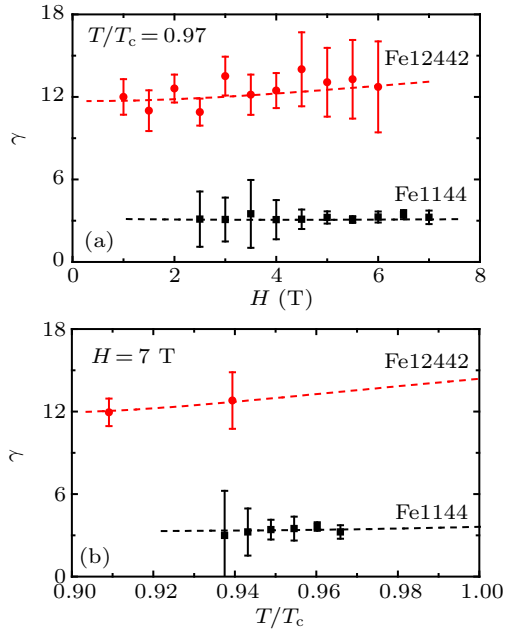



**Fig. 4.** Anisotropy parameters $\gamma$ of Fe1144 and Fe12442 obtained from torque measurements. (a) $H$ dependence of $\gamma$ at the reduced temperature $T/T_c = 0.97$. (b) $T$ dependence of $\gamma$ for $H = 7$ T. Error bars are the uncertainty of fit and the dash lines are guide to the eyes.

On the other hand, the irreversible part $\tau_{irr}$ is related to $J_c$,[39,40] that is,

$$J_c(H) = 3\tau_{irr}/rVH\sin\theta, \tag{4}$$

where $V$ is the volume of the single crystal and $r$ is sample's diameter (given that the sample has a cylinder shape, $V = \pi r^2 d$, $d$ is the thickness of the single crystal). For two-dimensional (2D) superconductors, Abrikosov lattice is only related to the perpendicular component of the magnetic field ($H\cos\theta$).[51] Then the critical current density in 2D regime can be expressed as $J_c(\theta, H) = J_c(H\cos\theta)$.[39] Thus it is convenient to plot $J_c$ vs. $H\cos\theta$. Figure 5(a) shows $H\cos\theta$ dependence of $J_c$ measured at temperature $T/T_c$ = 0.97 under different fields. The solid squares are the $J_c$ from the torque measurements while the solid stars from magnetization measurements in previous report.[20] And the hollow circles are data for Fe12442. It is found that the $J_c$s measured at different $H$ do not scale with each other but show a decreasing tendency with the increase of $H$. It suggests that Fe1144 is not a 2D superconductor in consistent with the fact that $\gamma \approx 3$. $J_c$ measured at $H = 2$ T is roughly comparable with the value from previous report,[20] (the small deviation may be caused by differences of the measure method and sample's shape), suggesting that the $J_c$ calculated based on Eq. (4) is reasonable. Note that, $J_c$ of Fe12442 is located at the bottom left corner of Fig. 5(a), suggesting a much lower critical current density as compared with Fe1144. Similar results can be found in Fig. 5(b), where $J_c$ is measured at different reduced temperature ($T/T_c$) and $H = 7$ T. The solid stars are data measured at $T = 33$ K with $T/T_c = 0.938$ from the previous magnetization measurements,[20] which are close to our data measured at the same $T/T_c$. It is also found that $J_c$ in Fe1144 at the investigated ranges is much higher than that in Fe12442 (hollow circles) at lower reduced $T/T_c$. Therefore, vortex pinning in Fe1144 is much stronger than that in Fe12442. The high $J_c$ in Fe1144 was interpreted in terms of the unique defect structure which leads to the advantageous vortex pinning properties.[20] While according to the discussion above, the interlayer interaction may also involve in vortex pinning in Fe1144 and Fe12442.

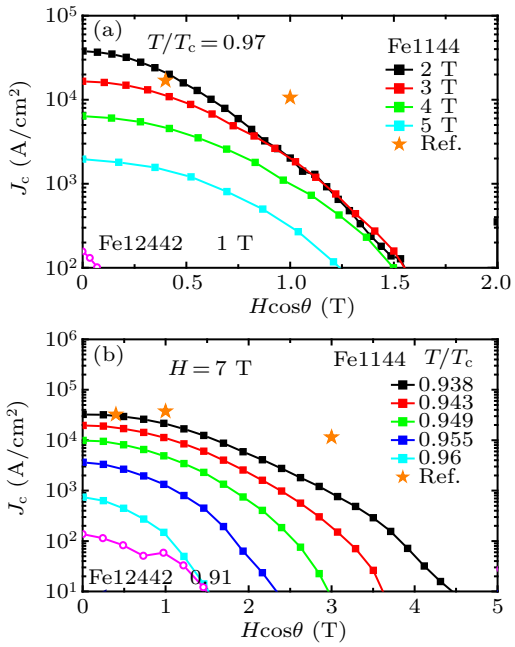



**Fig. 5.** The critical current density $J_c$ of Fe1144 (solid squares) and Fe12442 (hollow circles) as a function of $H\cos\theta$ at $T/T_c = 0.97$ (a) and $H = 7$ T (b). Solid stars are data taken from Ref. [20].

## 4. Conclusion

In summary, we have presented a detailed electrical transport and angular dependent torque investigation on Fe1144 and Fe12442 single crystals. In the resistance measurements, the anisotropy parameter of upper critical field $\gamma$ around $T_c$ of Fe1144 is about 3, which is clearly smaller than that of Fe12442 ($\gamma \approx 15$). By transforming resistance–temperature

($R$–$T$) curves to the Arrhenius plots, we find that Fe1144 has a larger activation energy than Fe12442. In combination with the literature data, we conclude that the FeSC with a smaller anisotropy exhibits a stronger vortex pinning. The magnetic torque measurements further confirm this result. At temperature $T \to T_c$, $\gamma \approx 3$ for Fe1144 and $\gamma \approx 15$ for Fe12442 are obtained by fitting reversible torque using the Kogan's model. Besides, the critical current density in Fe1144 is much higher than that in Fe12442 at the same reduced temperature and magnetic field. Our results suggest that the interlayer interaction may also take action on vortex pinning in FeSCs.

## Appendix A

The obtained TAFF energies of two single crystals at different magnetic fields are summarized in Fig. A1. We find that TAFF energy $U/k_B$ (solid points) ranges from 22671 K to 5202 K for Fe1144, which is a little larger than the $U/k_B$ calculated from previous report for Fe1144 (hollow points).[52] The value of $U/k_B$ for Fe12442 single crystal (solid points) is ranging from 1661 K to 315 K, which is also a little larger than that of polycrystal (hollow points).[21] The difference of $U$ between our results and literature most likely results from the different disorder landscape, defect, and quality of different samples, e.g., our samples are single crystal while the sample in literature is polycrystal.

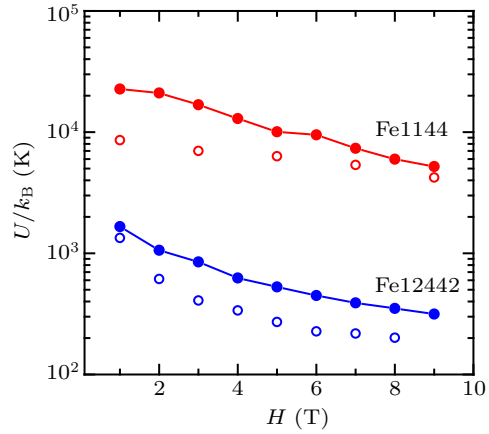



**Fig. A1.** The $H$ dependence of activation energy $U$ obtain from our data (solid points) and literature (hollow points). The blue and red hollows are the activation energy of Fe1144 single crystal[52] and Fe12442 polycrystal data,[21] respectively.

Nevertheless both of our data and literature show that the TAFF energy $U$ in Fe1144 is much larger than that in Fe12442. Thus our results suggest that the interlayer interaction may play a crucial role in vortex pinning in Fe12442 and Fe1144.

Figures A2(a)–A2(d) show the $\tau_{rev} = (\tau_{inc} + \tau_{dec})/2$ (empty circles) of Fe1144 and Fe12442, where the irreversible part has been masked, and the fitting results (solid lines) by Kogan's model[38] at different temperatures and magnetic fields.

Figures A3(a) and A3(b) show the $\tau_{irr} = (\tau_{inc} - \tau_{dec})/2$ of Fe1144 and Fe12442 at different temperatures and magnetic fields. Sharp peaks are observed around 90°, which are caused by the vortex pinning as the case of cuprate superconductor $Bi_2Sr_2CaCu_2O_x$.[39] Fe1144 shows a higher peak than Fe12442 at the same magnetic field and reduced $T/T_c$, suggesting that the vortex pinning in Fe1144 is stronger than that in Fe12442.

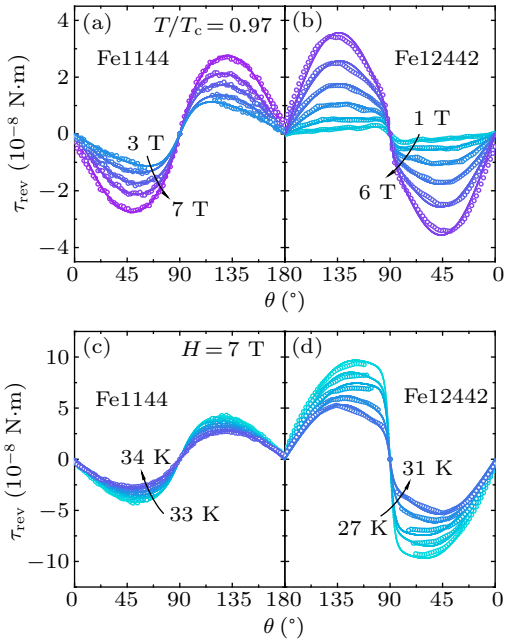



**Fig. A2.** The $\tau_{rev}$ (circles) and Kogan's model fitting curves (lines) at different temperatures and magnetic fields of $CaKFe_4As_4$ [(a) and (c)] and $KCa_2Fe_4As_4F_2$ [(b) and (d)].

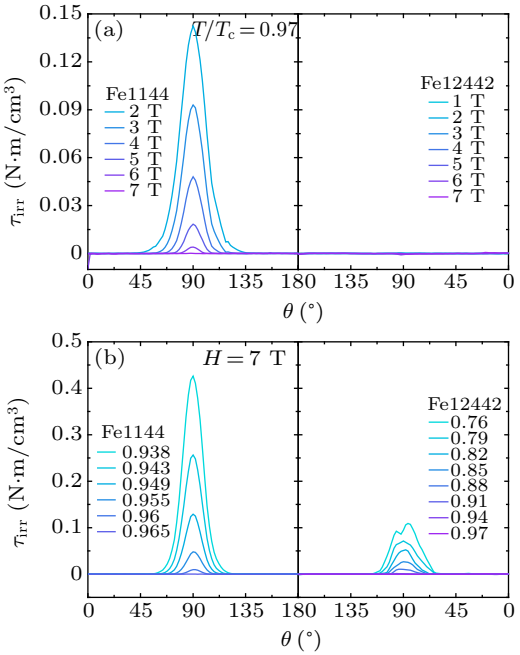



**Fig. A3.** Irreversible torque $\tau_{irr}$ of $CaKFe_4As_4$ and $KCa_2Fe_4As_4F_2$ as a function of angle $\theta$ measured at $T/T_c = 0.97$ for different magnetic fields (a) and $H = 7$ T for different temperatures (b).

## References

[1] Blatter G, Feigel'man M V, Geshkenbein V B, Larkin A I and Vinokur V M 1994 *Rev. Mod. Phys.* **66** 1125
[2] Bugoslavsky Y, Cohen L, Perkins G, Polichetti M, Tate T, Gwilliam R and Caplin A 2001 *Nature* **411** 561

[3] MacManus-Driscoll J, Foltyn S, Jia Q, Wang H, Serquis A, Civale L, Maiorov B, Hawley M, Maley M and Peterson D 2004 *Nat. Mater.* **3** 439

[4] Matsumoto K and Mele P 2009 *Superconductor Science and Technology* **23** 014001

[5] Lee S, Tarantini C, Gao P, *et al.* 2013 *Nat. Mater.* **12** 392

[6] Eisterer M 2017 *Superconductor Science and Technology* **31** 013001

[7] Leroux M, Kihlstrom K J, Holleis S, *et al.* 2015 *Appl. Phys. Lett.* **107** 192601

[8] Yuan P, Xu Z, Wang D, Zhang M, Li J and Ma Y 2016 *Superconductor Science and Technology* **30** 025001

[9] Blatter G, Geshkenbein V, Larkin A and Nordborg H 1996 *Phys. Rev. B* **54** 72

[10] Choi J H, Kim M S, Lee S I, Lee S Y, Yang I S, Yakhmi J, Mandal J, Bandyopadhyay B and Ghosh B 1998 *Phys. Rev. B* **58** 538

[11] Kamihara Y, Hiramatsu H, Hirano M, Kawamura R, Yanagi H, Kamiya T and Hosono H 2006 *J. Am. Chem. Soc.* **128** 10012

[12] Kamihara Y, Watanabe T, Hirano M and Hosono H 2008 *J. Am. Chem. Soc.* **130** 3296

[13] Ma Y 2012 *Superconductor Science and Technology* **25** 113001

[14] Shimoyama J 2014 *Superconductor Science and Technology* **27** 044002

[15] Wang X L, Ghorbani S R, Lee S I, *et al.* 2010 *Phys. Rev. B* **82** 024525

[16] Iyo A, Kawashima K, Kinjo T, Nishio T, Ishida S, Fujihisa H, Gotoh Y, Kihou K, Eisaki H and Yoshida Y 2016 *J. Am. Chem. Soc.* **138** 3410

[17] Meier W R, Kong T, Kaluarachchi U S, *et al.* 2016 *Phys. Rev. B* **94** 064501

[18] Khasanov R, Meier W R, Bud'ko S L, Luetkens H, Canfield P C and Amato A 2019 *Phys. Rev. B* **99** 140507

[19] Singh S J, Bristow M, Meier W R, Taylor P, Blundell S J, Canfield P C and Coldea A I 2018 *Phys. Rev. Materials* **2** 074802

[20] Ishida S, Iyo A, Ogino H, *et al.* 2019 *npj Quantum Mater.* **4** 27

[21] Wang Z C, He C Y, Wu S Q, Tang Z T, Liu Y, Ablimit A, Feng C M and Cao G H 2016 *J. Am. Chem. Soc.* **138** 7856

[22] Wang T, Chu J, Feng J, *et al.* 2020 *Sci. China Phys. Mech. Astron.* **63** 297412

[23] Wu D, Hong W, Dong C, *et al.* 2020 *Phys. Rev. B* **101** 224508

[24] Xu B, Munzar D, Dubroka A, Sheveleva E, Lyzwa F, Marsik P, Wang C, Wang Z, Cao G and Bernhard C 2020 *Phys. Rev. B* **101** 214512

[25] Hong W, Song L, Liu B, *et al.* 2020 *Phys. Rev. Lett.* **125** 117002

[26] Wang T, Zhang C, Xu L, *et al.* 2020 *Sci. Chin. Phys. Mech. Astron.* **63** 227412

[27] Yu A, Wang T, Wu Y, Huang Z, Xiao H, Mu G and Hu T 2019 *Phys. Rev. B* **100** 144505

[28] Meier W R, Kong T, Bud'ko S L and Canfield P C 2017 *Phys. Rev. Materials* **1** 013401

[29] Wang T, Chu J, Jin H, *et al.* 2019 *J. Phys. Chem. C* **123** 13925

[30] Jia Y, Cheng P, Fang L, Luo H, Yang H, Ren C, Shan L, Gu C and Wen H H 2008 *Appl. Phys. Lett.* **93** 032503

[31] Tinkham M 2004 *Introduction to Superconductivity*, 2nd edn. (New York: Courier Corporation)

[32] Zhou W, Zhuang J, Yuan F, Li X, Xing X, Sun Y and Shi Z 2014 *Appl. Phys. Express* **7** 063102

[33] Fang M, Yang J, Balakirev F, Kohama Y, Singleton J, Qian B, Mao Z, Wang H and Yuan H 2010 *Phys. Rev. B* **81** 020509

[34] Yuan H, Singleton J, Balakirev F, Baily S, Chen G, Luo J and Wang N 2009 *Nature* **457** 565

[35] Wang X, Ghorbani S, Dou S, Shen X L, Yi W, Li Z C and Ren Z A 2008 *arXiv preprint arXiv:0806.1318*

[36] Van Gennep D, Hassan A, Luo H and Abdel-Hafiez M 2020 *Phys. Rev. B* **101** 235163

[37] Wang Z, Xie T, Kampert E, Förster T, Lu X, Zhang R, Gong D, Li S, Herrmannsdörfer T, Wosnitza J and Luo H 2015 *Phys. Rev. B* **92** 174509

[38] Kogan V 1988 *Phys. Rev. B* **38** 7049

[39] Drzazga Z, Szymczak H and Szymczak R 1992 *Physica C* **203** 335

[40] Hagen C, Bom M, Griessen R, Dam B and Veringa H 1988 *Physica C* **153** 322

[41] Campbell L, Doria M and Kogan V 1988 *Phys. Rev. B* **38** 2439

[42] Kasahara S, Shi H, Hashimoto K, *et al.* 2012 *Nature* **486** 382

[43] Okazaki R, Shibauchi T, Shi H, Haga Y, Matsuda T, Yamamoto E, Onuki Y, Ikeda H and Matsuda Y 2011 *Science* **331** 439

[44] Sefat A S, Jin R, McGuire M A, Sales B C, Singh D J and Mandrus D 2008 *Phys. Rev. Lett.* **101** 117004

[45] Xiao H, Gao B, Ma Y, Li X, Mu G and Hu T 2016 *J. Phys.: Condens. Matter* **28** 325701

[46] Xiao H, Hu T, Zhang W, Dai Y, Luo H, Wen H, Almasan C and Qiu X 2014 *Phys. Rev. B* **90** 214511

[47] Xiao H, Hu T, Almasan C, Sayles T and Maple M 2006 *Phys. Rev. B* **73** 184511

[48] Ishida T, Okuda K, Asaoka H, Kazumata Y, Noda K and Takei H 1997 *Phys. Rev. B* **56** 11897

[49] Tachiki M and Takahashi S 1989 *Solid State commun.* **72** 1083

[50] Tachiki M and Takahashi S 1989 *Solid State commun.* **70** 291

[51] Kes P, Aarts J, Vinokur V and Van der Beek C 1990 *Phys. Rev. Lett.* **64** 1063

[52] Wang C, He T, Han Q, Wang B, Xie R, Li Y, Tang Q, Li Y and Yu B 2020 *Superconductor Science and Technology* **33** 045011